Structure and stability of bent core liquid crystal fibers

C. Bailey,[1] E. C. Gartland, Jr.,[2] and A. Jákli[1]
[1]*Chemical Physics Interdisciplinary Program and Liquid Crystal Institute, Kent State University, Kent, Ohio 44242, USA*
[2]*Department of Mathematical Sciences, Kent State University, Kent, Ohio 44242, USA*
(Received 24 October 2006; revised manuscript received 8 December 2006; published 5 March 2007)

Recently it was found that fluid smectic phases of bent core liquid crystals formed freestanding fibers of extremely high slenderness ratios. Studies of these fibers showed that their structure was composed of concentric cylindrical smectic layers. For this configuration to be stable there must be an energy term that desires bending of the smectic layers. We show that an energy term that deals with the divergence of the dipolar direction can encourage layer bending if the layer chirality value is allowed to vary. The energy term associated with holding the layer chirality is closely related to layer compressions and electrical self-interactions. For our model, we assumed a simple smectic-C geometry with constant molecular tilt and cone angle defined by the director with respect to the layer normal, but allowed a constant variation of the polar direction about the director. Applying this simplified model to a free energy which accounts for director distortions, divergence of the polar direction, biaxial layer strain, surface tension, and electrical self-interactions, we were able to show consistency between the stable fiber radius and other properties predicted in our model to results from experimental studies.

DOI: 10.1103/PhysRevE.75.031701 PACS number(s): 61.30.Cz, 64.70.Md, 61.30.Gd, 81.05.Lg

I. INTRODUCTION

Fiber formation ranges from natural processes such as silk drawn from spiders and silkworms to synthetic processes (for fiber formation) used in the production of nylon and polyester fabrics, optical fibers, and even body armor [1]. All of these are created by forming rigidity in the pulling process that opposes the constricting effects of surface tension. This rigidity can have various sources, such as a glassy transition under cooling to the evaporation of solvents or polymerization during the pulling process. Some of the earliest studies of liquid crystal fibers appeared in columnar liquid crystals and were possible due to the one dimensionality of the liquid [2]. Fiber stability for columnar liquid crystals was associated with a compression term dealing with the increase of column density perpendicular to the fiber direction [1,3], so while the surface tension would try to decrease the fiber's radius, the compression term would resist it. Estimation of the minimum stable fiber radius for columnar liquid crystals was calculated using the modified Plateau-Rayleigh (MPR) instability which tested the stability of the fiber to diameter fluctuations along the fiber length, and it was found that fibers are stable to all fluctuations for radii greater than R_m [4]:

$$R_m = \sigma/2B. \tag{1}$$

Here $\sigma \sim 0.03$ N/m is the surface tension and $B \sim 10^5$ N/m^2 is a compression modulus, thus giving $R_m \sim 0.15$ μm [1]. This value is actually about one order smaller than that observed experimentally.

The study of bent core liquid crystal fibers is fairly new, and much is unknown about their structure and properties. The presence of helical filaments growing in the bent core liquid crystal B_7 phase was first reported in 1999, where it was pointed out that polarization might have a crucial roll in the formation of the helical filaments [5,6]. There were also reports that the B_7 phase actually prefers to form stable fibers rather than stable thin films [5,7]. Characterization of the helical filaments indicated that they were composed of cylindrically concentric smectic layers and that the helicity was connected to the chiral symmetry breaking of the achiral molecules [8,9]. Studies of freestanding fibers showed that two bent core liquid crystal phases formed the most stable fibers and were identified to be the B_2 and B_7 phases [4]. The B_7 phase preferred to form single stable fibers in a very narrow size range with radii between 1.5 and 2 μm, while the B_2 phase could only form fibers of much larger radii [4], which could be associated to bundling of these smaller fiber units [4,10,11]. Interesting electrical properties of the fibers, such as repulsion and attraction to transverse electrical fields, push-pull attraction of bulk material to longitudinal electric fields, and fiber breaking to dc electric field pulses, point towards a charged behavior consistent with C_1 symmetry (i.e., polarization components both normal and parallel to the smectic layer normal) [4,12]. Using mechanical oscillations [10] and tensile force [12] measurements, the surface tension of bent core fibers has been measured to be about 25 mN/m. In measurements of the mechanical oscillations, a bulk energy term $\xi \sim 5$ kPa was measured [12] that contributed to the restoring force of the oscillating fiber. This term depended on the concavity of the fiber and was proportional to the volume, but its source was unknown.

The first theoretical explanation of bent core fiber stability used the same MPR argument used for columnar liquid crystals [see Eq. (1)] [4]. Just as for columnar liquid crystals, it also gives about one order of magnitude smaller radius than observed experimentally. Although it is tempting to explain this discrepancy by assuming that defects weaken the structure of the fibers and push this threshold radius (R_m) to larger values, in this case one would observe fibers in a wide range of radii, depending on the number of defects, which would vary from fiber to fiber. Experiments, however, clearly show discrete stable fiber diameters, thus suggesting that another mechanism stabilizes the fibers at radii over a micrometer.

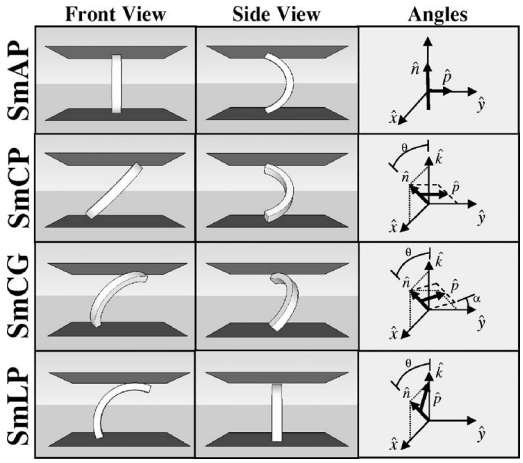

FIG. 1. Illustration of the molecular orientation of the molecular long axis $\hat{n}$ and the polarization direction $\hat{p}$ with respect to the smectic layer normal $\hat{k}$. In the SmAP phase, the long axis is parallel to the layer normal direction, while the polarization direction can be defined by an angle α about the director. The SmCP phase is defined by a constant tilt angle θ, and the polarization direction is bound to the layer (xy) plane. In the SmCG phase, the orientation can be identified by a layer tilt angle θ and a polarization angle α forming the most general molecular orientation of the three. In the SmLP phase the polarization lies in the tilt plane defined by the molecular long axis and the smectic layer normal.

Here we propose a theoretical model that explains the source of bent core liquid crystal fiber stability and connects it to the molecular and phase structures of the constituent materials.

II. THE MODEL

Our study probes fiber stability on three major bent core phases: the SmAP, SmCP (B_2), and the SmCG. Previous theoretical considerations of these phases were laid out by Brand, Cladis, and Pleiner in 1998, in which they discussed the symmetries and possible macroscopic consequences of these phases [13]. The basic molecular orientations with respect to the undistorted layer normal for these phases are sketched in Fig. 1 and can be fully described by two angles θ and α. In all of the phases, we see three important directions described by the layer normal $\hat{k}$, the director direction $\hat{n}$, and the polar direction $\hat{p}$ which must be perpendicular to the director to hold the head-tail symmetry.

In the SmAP phase, there exists a twofold symmetry axis along two mirror planes (C_{2v}). It is a polar phase where the polar direction $\hat{p}$ is perpendicular to layer normal $\hat{k}$, which is parallel to the director $\hat{n}$. SmAP materials show in-plane birefringence and ferroelectric or antiferroelectric type switching [14].

The SmCP phase is also polar parallel to the layer plane, but the molecular plane is tilted with respect to the layer normal. This phase is interesting because of the formation of distinct chiral domains even though the molecules are achiral [7]. The smectic layers have a twofold rotational symmetry (C_2) about the polar direction, and the chirality arises from broken mirror symmetry induced by the coupling of layer tilt and polarization.

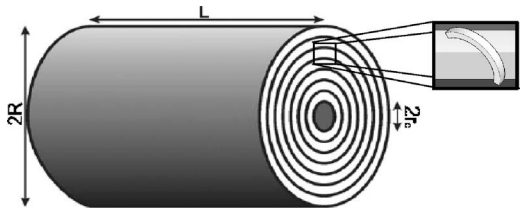

FIG. 2. The fiber geometry used in our stability analysis. The fiber has length L, outer radius R, and inner cutoff radius r_c, where the smectic properties are assumed to break down. This model shows the layered structure consisting of concentric smectic layers which are essential for fiber stability.

The B_7 structures are characterized by helical superstructures, such as telephone-cord-like filaments formed while cooling from the isotropic fluid. Some of these structures cannot be switched by electric fields whereas others are switchable, suggesting different phase structures. The electric-field-induced optical and mechanical behavior of these switchable B_7 materials can be consistently explained by a double tilted structure with C_1 symmetry [15]. X-ray and freeze fracture studies of nonswitchable B_7 materials, however, indicate a polarization modulated $(B_{7-\mathrm{mod}})$ [16] or even a digitized smectic structure that can be interpreted as a columnar phase composed of smectic ribbons. On the other hand, we do not see any evidence in the literature which would rule out local C_1 symmetry (i.e., double-tilted director structure in the smectic ribbons) of these original B_7 materials. In our model we will consider the SmCG model, and we will find that a double tilted structure with $\alpha \neq 0, \pi$ stabilizes the formation of fibers and filaments.

The SmLP phase can be called the "leaning" smectic phase and results from the polarization direction lying along the tilt plane. Although this phase has never been found experimentally it has theoretical importance, since this provides the largest out-of-layer polarization for a given layer tilt.

Regarding their fiber stability, our experiments showed that SmAP materials do not form stable fibers; SmCP can form both films and bundle of fibers, whereas the B_7 materials form single and bundles of fibers, but they do not form freestanding films.

Throughout our model, we assume a very simple smectic structure consisting of concentric cylindrical layers running through the entire length of the fiber (L) and from the outer radius (R) of the fiber to some defect core radius (r_c). This very simple model is shown in Fig. 2, and although not noted in the figure, the cylindrical coordinate system that we will be working in is as follows: $\hat{r}$ pointing radial from the fiber center, $\hat{z}$ pointing along the fiber long axis, and $\hat{\psi}$ being mutually perpendicular to $\hat{r}$ and $\hat{z}$ such that $\hat{r} \times \hat{\psi} = \hat{z}$. With this coordinate system, we assume that the smectic layer normals lie along the radial coordinate $\hat{r}$.

Although the geometry is simple, we allow the formation of the general double-tilted SmCG phase characterized by nonzero polar and azimuthal angles α and θ, respectively.

For the sake of simplicity, we fix the tilt angle θ and assume that it cannot be changed by external fields. We also assume that the polarization angle α is constant and independent of the radial position, though we allow its uniform variation under external fields. The azimuth angle is set to a constant along the $r\psi$ plane for simplicity and because previous experimental studies warranted this geometry [4]. With these constraints, we can define the molecular long axis $\hat{n}$ (director), the polarization direction $\hat{p}$, and the molecular plane normal $\hat{m}$ in terms of these angles:

$$\hat{n} = \cos\theta\hat{r} + \sin\theta\hat{\psi}, \tag{2}$$

$$\hat{p} = \sin\theta\sin\alpha\hat{r} - \cos\theta\sin\alpha\hat{\psi} + \cos\alpha\hat{z}, \tag{3}$$

$$\hat{m} = \sin\theta\cos\alpha\hat{r} - \cos\theta\cos\alpha\hat{\psi} - \sin\alpha\hat{z}. \tag{4}$$

By using $\hat{n}$ and $\hat{p}$, we can define the chiral order parameter χ of the layers as [17]

$$\chi = 2(\hat{r}\times\hat{n}\cdot\hat{p})(\hat{r}\cdot\hat{n}) = \sin 2\theta\cos\alpha. \tag{5}$$

The layers have maximum chirality when $\cos\alpha = \pm 1$, corresponding to the SmCP phase. For $0 < |\chi| < \sin 2\theta$, then the layers have C_1 symmetry (SmCG phase). When $|\chi| = 0$, this phase has C_s symmetry (SmLP phase), and if the tilt plane lies in the rψ plane, then distortions of the layers do not break the C_s layer symmetry.

Taking into account both the bulk and surface free energies, the total free energy $F(R,\alpha)$ can be obtained by integrating the free energy density $f_B(r,\alpha)$ over a cylindrical volume and the surface energy density $S(\alpha)$ over the surface area:

$$F(R,\alpha) = 2\pi L\int_{r_c}^{R} f_B(r,\alpha)r\,dr + 2\pi LRS(\alpha). \tag{6}$$

Then by dividing by $2\pi L$, we can obtain the free energy per length $\Phi(R,\alpha)$ as

$$\Phi(R,\alpha) = \frac{F(R,\alpha)}{2\pi L} = \int_{r_c}^{R} f_B(r,\alpha)r\,dr + RS(\alpha). \tag{7}$$

Obviously, when the energy minimum occurs at $R = r_c$, then the bulk terms disappear and the surface term which is governed by surface tension dominates forcing the fiber to break. However, if the minimum occurs when $R > r_c$, then the bulk energy may overcome the cost of the surface tension and fiber stability can be achieved.

A. Bulk energy terms

1. Director distortions

This energy density accounts for the low-energy (Frank free energy [1,18]) distortions of the director field in the smectic system. Using the one-constant approximation for the distortion elastic constant K and ignoring the K_{24} term, our energy density takes the classical form [18]

$$F_N(R) = \frac{1}{2}K[(\vec{\nabla}\cdot\hat{n})^2 + (\vec{\nabla}\times\hat{n})^2] = \frac{1}{2}K\frac{1}{r^2}. \tag{8}$$

The energy density from this term integrates out to have a logarithmic relationship to the core radius r_c as

$$\Phi_N(R) = \frac{1}{2}K\ln\left(\frac{R}{r_c}\right). \tag{9}$$

Below r_c, the director distribution does not matter, and the material is assumed to be either isotropic or a nematic fluid whose director points along the fiber and is undistorted.

2. Dipolar divergence distortions

Linear divergence of the dipolar direction may contribute to the free energy via two mechanisms: elastic (molecular packing) and electrostatic interactions:

$$f_D = c'(\vec{\nabla}\cdot\hat{p}) + c''(\vec{\nabla}\cdot\vec{P}) \approx (c' + c''P_0)(\vec{\nabla}\cdot\hat{p}) = C_{\text{eff}}(\vec{\nabla}\cdot\hat{p}). \tag{10}$$

The first term has an energy constant c' and is entirely elastic in nature and can be determined from maximizing the molecular packing. The second term has an energy constant c'' and is related to electrostatic repulsion of a macroscopic polarization $\vec{P}$ along $\hat{p}$. Furthermore, if the total polarization magnitude P_o is constant, we can define an effective energy constant C_{eff} which is a linear combination of the two effects. Although we combine c' and c'' in the C_{eff} term, the need to separate these two mechanisms is essential because the elastic c' term is independent of all other energy terms and only drives splay of the molecular kink directions; however, the electrostatic c'' term is proportional to the macroscopic polarization which is present in other energy terms such as the electric self-interactions.

Using the notation provided in Eq. (10), we can easily rewrite the dipolar divergence free energy density f_D and free energy per length Φ_D in terms of the angles θ and α:

$$f_D(r,\alpha) = C_{\text{eff}}(\vec{\nabla}\cdot\hat{p}) = C_{\text{eff}}\sin\theta\sin\alpha(1/r), \tag{11}$$

$$\Phi_D(R,\alpha) = C_{\text{eff}}\sin\theta\sin\alpha(R - r_c). \tag{12}$$

The signs of c' and c'' can be positive or negative depending on their molecular properties, but Eq. (12) can always be negative by changing the sign of α, so Φ_D can always oppose the effects of surface tension. Furthermore, Φ_D is also proportional to the fiber radius and has a tilt angle dependence which eliminates this term in the SmAP phase where $\theta = 0$.

3. Electric self-interactions

This energy density has three components: the first term deals with dielectric interactions with electric fields $\vec{E}_i$ created by the diverging spontaneous polarization, the second term takes into account the dielectric interactions with externally applied electric fields $\vec{E}_e$, and the last term describes the interaction between the spontaneous polarization and both internal and external fields:

$$f_E = \frac{1}{2}\vec{D}_i \cdot \vec{E}_i - \frac{1}{2}\vec{D}_e \cdot \vec{E}_e - \vec{P} \cdot (\vec{E}_i + \vec{E}_e). \tag{13}$$

The first and second terms have opposite signs because the first is due to fields generated by constant charge and the second arises from constant potential. In order to use a more convenient form, we will add and subtract a term of the form $1/2\varepsilon_o(\vec{E}_i+\vec{E}_e)\cdot(\vec{E}_i+\vec{E}_e)$, where ε_o is the dielectric permittivity of free space. By regrouping the terms we can obtain the following equation, where $\bar{\varepsilon}$ is the relative dielectric tensor and $\bar{I}$ is the identity matrix:

$$f_E = \frac{1}{2}\varepsilon_0(\bar{\varepsilon}-\bar{I})\vec{E}_i \cdot \vec{E}_i - \frac{1}{2}\varepsilon_0(\bar{\varepsilon}-\bar{I})\vec{E}_e \cdot \vec{E}_e - \vec{P} \cdot (\vec{E}_i + \vec{E}_e) + \frac{1}{2}\varepsilon_0(E_i^2 - E_e^2). \tag{14}$$

This form of the equation is useful because it shows that the first and second terms are just interactions between the induced polarization $\vec{P}_{\text{ind}}=\varepsilon_o(\bar{\varepsilon}-\bar{I})\vec{E}$ and the electric fields surrounding them. The last term deals with the effects of electric fields in the absence of the dielectric material and occurs in all space, while the others act only within the fiber. For our current model we will be ignoring the effects of external fields and consider only electric self-interactions. This reduces Eq. (14) to the following:

$$f_E = \frac{1}{2}\varepsilon_0(\bar{\varepsilon}-\bar{I})\vec{E}_i \cdot \vec{E}_i - \vec{P} \cdot \vec{E}_i + \frac{1}{2}\varepsilon_0 E_i^2. \tag{15}$$

Finally we will neglect the last term outside of the fiber because in the real system there will exist free charges which can drastically limit the effects of electric fields outside of the fiber.

This form of the equation is useful to us for two reasons: first, it limits the volume of integration to that of the fiber and does not extend over all space; second, it allows us to inspect the effects of the self interacting fields. Luckily, due to the simple geometry of our model, we are able to derive the internal electric field by using Gauss's law inside the fiber:

$$\int\int \varepsilon_0 \bar{\varepsilon}\vec{E}_i \cdot d\vec{A} = -\int\int\int (\vec{\nabla}\cdot\vec{P})dV,$$

$$\int\int \varepsilon_0 \bar{\varepsilon}_{rr} E_i r\, d\theta\, dz = -P_0 \sin\theta \sin\alpha \int\int\int \left(\frac{1}{r}\right) r\, dr\, d\theta\, dz,$$

$$\varepsilon_0 \bar{\varepsilon}_{rr} E_i r = -P_0 \sin\theta \sin\alpha (r - r_c),$$

$$\vec{E}_i = -\frac{P_0(\bar{\varepsilon}_{rr})^{-1}}{\varepsilon_0} \sin\theta \sin\alpha \left(1 - \frac{r_c}{r}\right)\hat{r}. \tag{16}$$

This can be calculated exactly because over all other dimensions except in the $\hat{r}$ direction, we assumed that the polarization does not diverge and cannot form fields. Therefore only the radial component of the electric field will exist, which makes it an excellent candidate for this technique. Then by plugging the results from Eqs. (16) for the internal electric field into the reduced form of the free energy density (15), we are able to obtain the free energy density and free energy per length in terms of θ and α:

$$f_E(r,\alpha) = \frac{P_0^2(\bar{\varepsilon}_{rr})^{-1}}{\varepsilon_0}(\sin\theta\sin\alpha)^2\left[\frac{1}{2}\left(\frac{r_c}{r}\right)^2 - 2\frac{r_c}{r} + \frac{3}{2}\right], \tag{17}$$

$$\Phi_E(R,\alpha) = \frac{P_0^2(\bar{\varepsilon}_{rr})^{-1}}{\varepsilon_0}(\sin\theta\sin\alpha)^2\left[\frac{1}{2}r_c^2 \ln\left(\frac{R}{r_c}\right) - 2r_c(R-r_c) + \frac{3}{4}(R^2 - r_c^2)\right]. \tag{18}$$

The inverse of the relative dielectric tensor appears in both Eqs. (17) and (18). This term operates only in the $\hat{r}$ direction and therefore is reduced to a single element of the inverse tensor. This can be calculated by

$$(\bar{\varepsilon}_{rr})^{-1} = \frac{1}{\varepsilon_1}(\hat{n}\cdot\hat{r})^2 + \frac{1}{\varepsilon_2}(\hat{m}\cdot\hat{r})^2 + \frac{1}{\varepsilon_3}(\hat{p}\cdot\hat{r})^2 = \frac{1}{\varepsilon_1}\cos^2\theta + \frac{1}{\varepsilon_2}\sin^2\theta\cos^2\alpha + \frac{1}{\varepsilon_3}\sin^2\theta\sin^2\alpha, \tag{19}$$

where ε_1, ε_2, and ε_3 are the eigenvalues of the dielectric tensor in the molecular frame of reference.

4. Layer compression

Although our model assumes a constant tilt angle, which for rod-shaped molecules would be equivalent to the layer incompressibility condition, such is not the case here, where we allow changes of α—i.e., the change of layer chirality. To account for this in our model, we will use the classical layer compression free energy density:

$$f_C = \frac{1}{2}B\gamma^2 \approx \frac{1}{2}B\left(\frac{d-d_0}{d_0}\right)^2, \tag{20}$$

where B is the layer compression modulus and γ is the layer strain, which accounts for variations of the layer thickness d from that of its equilibrium value d_o. In order to take into account the effects of changing the layer chirality, we must introduce a new type of layer thickness. To describe bent core molecules having a three-dimensional shape, we define the shape tensor $\bar{D}$ as

$$\bar{D}_{\text{mol}} = \begin{pmatrix} d_1 & 0 & 0 \\ 0 & d_2 & 0 \\ 0 & 0 & L \end{pmatrix}, \tag{21}$$

where d_1, d_2, and L are the molecular dimensions defined in Fig. 3.

The effective layer thickness (assuming rigid molecules) d changes when the polarization direction is varied as

$$d = (\bar{D}\hat{k})\cdot\hat{k}. \tag{22}$$

In Fig. 3, we see that changing the polarization direction can induce a minor change in the layer thickness, δ, which is

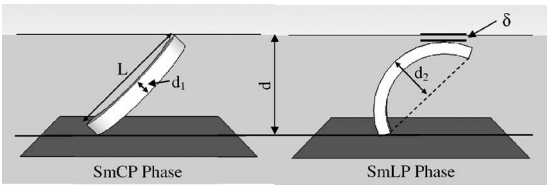

FIG. 3. A comparison of the layer thickness between the SmCP and SmLP phases where both molecules have a layer tilt of $\pi/4$. The SmCP phase has the polarization direction lying in the smectic layer; however, the SmLP phase has the polarization direction lying in the tilt plane. In both phases the layer spacing has been set to the distance for the SmCP phase and both molecules touch the bottom layer; however, the SmLP phase creates a small layer thickness change δ via the shape of the molecule.

dependent on the direction of the polarization with respect to the layer normal. Taking into account the angular variation of the molecular coordinate system with respect to the layer normal $\hat{k}$ defined by θ and α, we can express d as

$$d = d_1 + (L - d_1)\cos^2\theta + (d_2 - d_1)\sin^2\theta\sin^2\alpha. \quad (23)$$

What is interesting about Eq. (23) is that the angular dependences of d go with the square of the angles which does not bias the net layer chirality of the system (in both maximum chirality values $\sin\alpha = 0$). When this formalism is introduced into Eq. (20) along with the assumptions of constant tilt angle and $(d_2 - d_1)/(L - d_1) < 1$ and $d_1/(L - d_1) << 1$, we arrive at the following relationship:

$$\begin{aligned} f_C(\alpha) &= \frac{1}{2}B\left(\frac{d_1 + (L - d_1)\cos^2\theta + (d_2 - d_1)\sin^2\theta\sin^2\alpha}{d_1 + (L - d_1)\cos^2\theta_0 + (d_2 - d_1)\sin^2\theta_0\sin^2\alpha_0} - 1\right)^2 \\ &\approx \frac{1}{2}B\left(\frac{(d_2 - d_1)}{(L - d_1)}\tan^2\theta_0\right)^2(\sin^2\alpha - \sin^2\alpha_0)^2 \\ &= \frac{1}{2}B_{\text{eff}}(\sin^2\alpha - \sin^2\alpha_0)^2, \end{aligned} \quad (24)$$

where θ_o and α_o are the tilt and polar angles of the material at their unstrained positions. What is interesting about the polarization direction's effect on the compression modulus is an effective rescaling by a factor of about 5% assuming that $(d_2 - d_1)$ is approximately 1 nm and the length is about 5 nm.

$$\begin{aligned} B_{\text{eff}} &= B\left(\frac{d_2 - d_1}{L - d_1}\tan^2\theta_0\right)^2 \approx (10^5\ \text{Pa})\left(\frac{1\ \text{nm}}{4.5\ \text{nm}}\tan^2\frac{\pi}{4}\right)^2 \\ &\approx 5\ \text{kPa}. \end{aligned} \quad (25)$$

This allows us to obtain a bulk elastic energy term that could explain the unknown elastic energy term ξ measured by Stannarius *et al.* [12]. Furthermore, the free energy per length for this term would look like

$$\Phi_C(R,\alpha) = \frac{1}{4}B\left(\frac{d_2 - d_1}{L - d_1}\tan^2\theta_0\right)^2(\sin^2\alpha - \sin^2\alpha_0)^2(R^2 - r_c^2) \quad (26)$$

and would oppose the effects of curvature induced by Φ_D.

On a side note, similar terms to the energy density in Eq. (24) can be derived from elastic theory as long as it is invariant under $(\hat{n},\hat{k}) \leftrightarrow (-\hat{n},-\hat{k})$ inversion. One possible candidate takes the form of variations of the square of the layer chirality χ from its undistorted state χ_o:

$$f_C'(\alpha) = \frac{1}{2}B_c(\chi^2 - \chi_0^2)^2 = \frac{1}{2}B_c\sin^4 2\theta(\sin^2\alpha - \sin^2\alpha_0)^2. \quad (27)$$

From Eq. (27), we can see that the energy term in Eq. (24) holds the layer chirality constant when external stresses are not applied.

B. Surface term

The surface term provides an energy cost for creating an interface between two media, in our case air and liquid crystal. Assuming a biaxial tensor relationship for the surface tension $\bar{\sigma}$ which couples the orientation of the local molecular coordinate system $\hat{n}$, $\hat{m}$, and $\hat{p}$, to the surface normal $\hat{k}$, this energy density would take the following form:

$$S = (\bar{\sigma}\hat{k})\hat{k}. \quad (28)$$

In our geometry the surface normal is along $\hat{r}$, so we can rewrite Eq. (28) as

$$\begin{aligned} S(\alpha) &= \sigma_1(\hat{n}\cdot\hat{r})^2 + \sigma_2(\hat{m}\cdot\hat{r})^2 + \sigma_3(\hat{p}\cdot\hat{r})^2, \\ S(\alpha) &= \sigma_1\cos^2\theta + \sigma_2\sin^2\theta\cos^2\alpha + \sigma_3\sin^2\theta\sin^2\alpha. \end{aligned} \quad (29)$$

This results in a free energy per length

$$\Phi_S(R,\alpha) = R(\sigma_1\cos^2\theta + \sigma_2\sin^2\theta\cos^2\alpha + \sigma_3\sin^2\theta\sin^2\alpha). \quad (30)$$

C. Core energy term

To examine the possible effect of the core on fiber stability, we will overestimate its energy by assuming that the defect core has enough distortion energy to completely melt the liquid crystalline material in the core to the isotropic phase. This energy can be estimated by assuming that the fiber is in the liquid crystalline phase in thermal equilibrium at temperature T below the isotropic transition temperature T_o. Accordingly,

$$E_{\text{core}} < (nk_b(T_0 - T) + \rho H)V_{\text{core}}, \quad (31)$$

where n is the number density of the molecules, k_b is Boltzmann's constant, ρ is the mass density, H is the sum of specific latent heats of the liquid crystal phases to the isotropic phase, and V_{core} is the volume of the defect core. Assuming

TABLE I. List of simulated physical property values.

Variable	Description	Value
θ_o	Equilibrium smectic tilt angle	$-\pi/2<\theta_o<\pi/2$
α_o	Equilibrium polarization angle	$-\pi<\alpha_o<\pi$
r_c	Defect core radius	5×10^{-9} m
R	Outer fiber radius	10^{-8} m$<R<10^{-5}$ m
K	Director elastic constant	10^{-11} N
P_o	Spontaneous polarization	10^{-4} C/m$^2<P_o<10^{-1}$ C/m^2
c'	Elastic div. of dipole direction constant	0 N/m$<c'<$0.055 N/m
c''	Electric div. of dipole direction constant	0 V$<c''<$55 V
B	Layer compression modulus	10^5 Pa
$\frac{d_2\text{-}d_1}{L\text{-}d_1}$	Approximately the width to length ratio of the molecule	0.2
ε_1	Relative dielectric constant along $\hat{n}$	7
ε_2	Relative dielectric constant along $\hat{m}$	10
ε_3	Relative dielectric constant along $\hat{p}$	12
σ_1	Surface tension along $\hat{n}$	0.026 N/m
σ_2	Surface tension along $\hat{m}$	0.024 N/m
σ_3	Surface tension along $\hat{p}$	0.025 N/m

that the defect is a straight line running down the center of the fiber, the defect volume can be written as the volume of a cylinder of radius r_c and length L. By replacing the number density in (31) by the combination of mass density ρ, Avagadro's number N_A, and molar mass M, we can calculate the energy per length, Φ_{core}, by dividing (31) by a constant factor of $2\pi L$ as we did in Eq. (7), and plugging in reasonable values for the material properties we obtain

$$\Phi_{\text{core}} < \left[\left(\frac{\rho N_A}{M}\right)k_b(T_o - T) + \rho H\right]\frac{1}{2}r_c^2. \tag{32}$$

III. RESULTS

Now that we have derived all of the possible energy contributions, we can write the total energy per length as the sum of these components:

$$\Phi_{\text{total}}(R,\alpha) = \Phi_N(R) + \Phi_D(R,\alpha) + \Phi_E(R,\alpha) + \Phi_C(R,\alpha) + \Phi_S(R,\alpha) + \Phi_{\text{core}}. \tag{33}$$

This free energy has to be minimized for R and α for a given set of property values to find the equilibrium structure. Fiber stability for all lengths requires that the minimum of the energy per length be negative and the radius at this minimum be larger than r_c. To simulate the real situations as closely as possible, we have varied the parameters θ_o, α_o, R, c', c'', and P_o and have used reasonable fixed values for the remaining parameters. Both the ranges and the fixed values are provided in Table I.

Before proceeding with the numerical calculations we compare Φ_{core} with the other terms in Eq. (33) using the parameters given in Table I, furthermore assuming a 1-μm fiber with $\alpha_o=0$, $\alpha=-\pi/2$, $\theta_o=\pi/4$, $P_o=10^{-3}$ C/m^2, $c'=0.04$ N/m, $c''=11.2$ V, and a typical molecular weight of 800 g/mol. At 10 °C below the isotropic-smectic transition with a typical latent heat of 20 J/g we find from (32) that $\Phi_{\text{core}}\leqslant 2.51\times10^{-10}$ N. On the other hand, we find $\Phi_{\text{total}}=-4.85\times10^{-9}$ N, showing that by neglecting the defect term we introduce an error of less than 5%. Since the calculated core energy is an overestimate, it is justified to neglect it in our model. In any case, the core energy would mainly influence the stability transition range and not the stable fiber radius. We also note that the director distortion energy per length, $\Phi_N=2.65\times10^{-11}$ N, is even smaller than that of Φ_{core} and can be neglected as well.

With the remaining terms we would like to analyze the relationships between the total spontaneous polarization P_o, the divergence terms c' and c'', and the effects of varying θ_o and α_o on fiber stability.

Numerical results were obtained by minimizing the energy per length Φ_{total} with respect to R and α via a combination of derivative-free function minimization techniques provided in the Matlab Optimization Toolbox, such as golden section search and parabolic interpolation combined with unconstrained nonlinear optimization techniques such as the simplex search method. Combining these multiple techniques helps guarantee that a minimum solution to Eq. (33) can be obtained and that the solutions are not local minima or maxima.

Polarization dependences were studied by varying the polarization and calculating the stable fiber radius for three situations. The first numerical calculation sets $c'=0.04$ N/m and $c''=0$, which probe the behavior of purely elastic splay of the polarization. The second set $c''=11.2$ V and neglects c', which probes dipolar divergence effects. Finally we simulate the general case which uses C_{eff} with $c'=0.04$ N/m and $c''=11.2$ V and accounts for both sources of dipolar divergence (Fig. 4). What we see in this graph is that polarization has a tremendous effect on fiber stability. The energy cost due to electric self-interaction is extremely im-

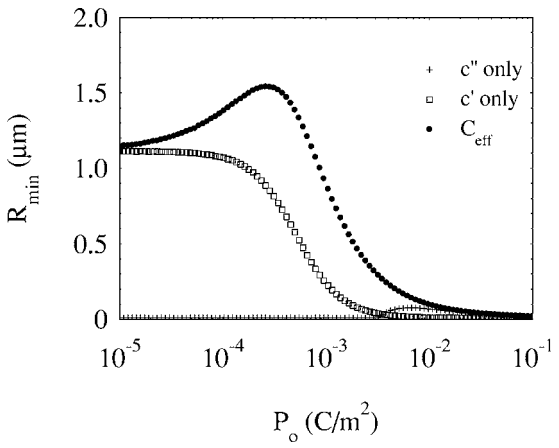

FIG. 4. Numerical results for the polarization dependence on fiber stability. Computations were performed on three situations for Φ_D; with c' only, c'' only, or C_{eff}, and the results show some insight into the mechanisms of fiber stability. The most striking difference between the curves is the polarization range at which each term dominates. The c' only term dominates at low polarizations while at larger polarizations, $P_o > 5\times10^{-4}$ C/m^2; the electric self-interaction begins to shrink the stable fiber radius. For the c''-only term, at low polarizations $P_o < 5\times10^{-3}$ C/m^2, fiber stability does not exist: however, above this value a transition occurs in which fibers can form. The C_{eff} term that takes both of these behaviors into account is stable over the entire range but dominates in the midranges between 10^{-4} C/m$^2 < P_o < 5\times10^{-3}$ C/m^2 and peaks at around 5×10^{-4} C/m^2.

portant in defining the stable fiber radius. This effect can be best seen in the c'-only curve which has a "damping" in the stable radius due only to electric self-interaction of Φ_E. The c'' curve has a strong stability transition and does not form

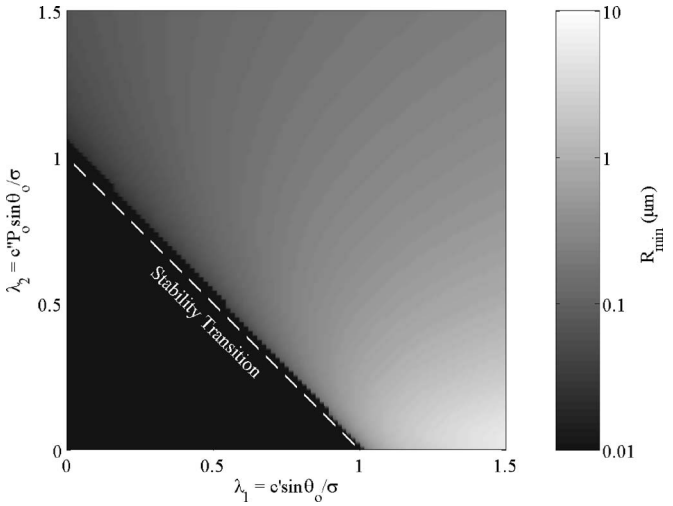

FIG. 5. Phase diagram which compares the effects of $\lambda_1 = c'\sin\theta_o/\sigma$ to $\lambda_2 = c''P_o \sin\theta_o/\sigma$ on fiber stability, where only P_o is varied in the calculation of λ_2 and c'' is set to 11.2 V. The different shading represents the stable fiber radius. A factor of $\sin\theta$ is introduced into λ_1 and λ_2 to correctly account for the maximum out-of-layer polarization that contributes to this effect. The stability threshold (dashed line) marks the boundary between stable and unstable fibers.

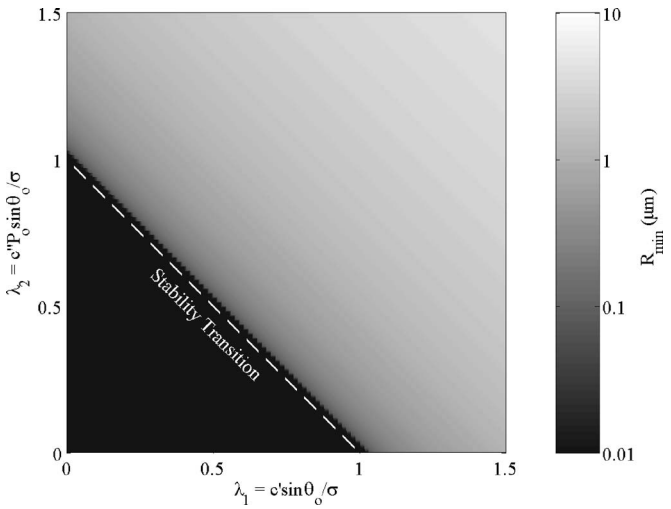

FIG. 6. Phase diagram which compares the effects of $\lambda_1 = c'\sin\theta_o/\sigma$ to $\lambda_2 = c''P_o \sin\theta_o/\sigma$ on fiber stability, Where only c'' is varied in the calculation of λ_2 and $P_o = 10^{-3}$ C/m^2. The shading represents the stable fiber radius.

very large stable fibers as compared to the c'. However, the presence of polarization amplifies the stable fiber radius in the C_{eff} curve and forms much more stable fibers. This leads us to the following conclusions: fiber stability is strongly related to the combined effects of c' and c'' especially when c' has a strength greater than the surface tension: otherwise, there will be a strong stability transition which arises from a competition between the c'' term and electric self-interaction greatly reducing fiber stability. Referring back to Sec. II A 2, we emphasize again that even though the c' and c'' are linearly combined, the resulting effect of the two mechanisms can be very different due to the c'' coupling to other energy terms.

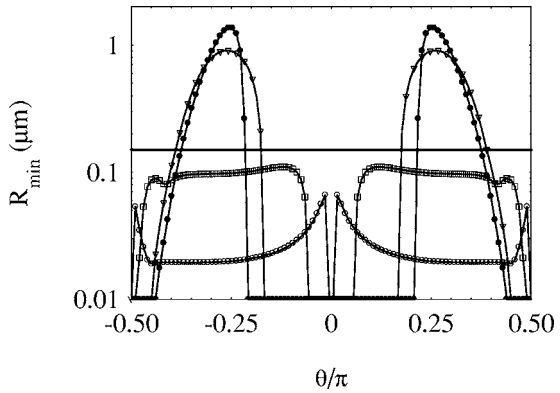

FIG. 7. The effects of tilt angle on the stable fiber radius for various polarizations: $P_o = 10^{-4}$ C/m^2 (●), $P_o = 10^{-3}$ C/m^2 (▽), $P_o = 10^{-2}$ C/m^2 (□), and $P_o = 10^{-1}$ C/m^2 (○), when $\alpha_o = 0$. We can see that for all polarizations in the SmAP phase ($\theta_o = 0$) there is no stable fiber with $r > r_c$. However, there is a definite threshold behavior that occurs which is strongly dependent on the polarization. Furthermore, we see that SmCP materials with larger polarizations ($P_o \approx 10^{-2}$ C/m^2) can form stable fibers, but their radius is below the MPR instability threshold (solid line), $R_m = 0.15$ μm, which would be unstable to longitudinal diameter fluctuations.

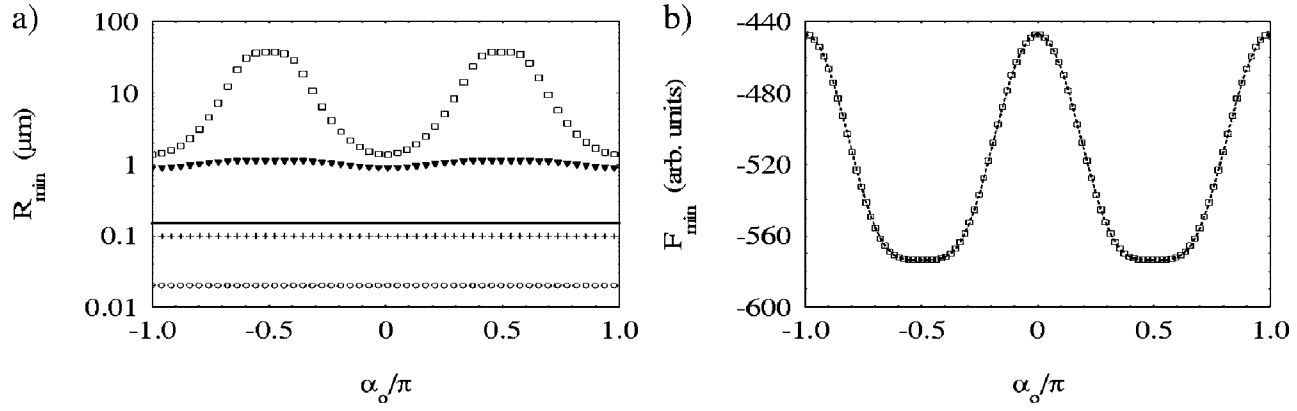

FIG. 8. (a) Plot of stable fiber radius versus the value of α_o at various polarization values: $P_o=10^{-4}$ C/m^2 (□), $P_o=10^{-3}$ C/m^2 (▼), $P_o=10^{-2}$ C/m^2 (+), and $P_o=10^{-1}$ C/m^2 (○). The bulk α_o value has a significant effect on the stable fiber radius for small polarizations; however, the corresponding stable radii are large. Larger polarizations also show this effect: however, their differences are much more constrained. The largest stable single fibers occur in the SmLP phase ($\alpha_o/\pi=0.5$) and decrease as we move through the SmCG phase and have a minimum in the SmCP phase. The MPR line (solid line) denotes the threshold from the modified Plateau-Rayleigh instability threshold, below which no fibers are stable. (b) The free energy per length for the $P_o=10^{-3}$ C/m^2 case with varying α_o, which shows that the free energy is minimized in the SmLP phase and has a maximum in the SmCP phase.

The effects of electric self-interactions can be seen more clearly in Fig. 5, which compares the effects of $\lambda_1=c'\sin\theta_o/\sigma$ and $\lambda_2=c''P_o\sin\theta_o/\sigma$ to the simulated stable fiber radius. What we see is that when $\lambda_1+\lambda_2<1$, denoted by the dashed line, then fiber stability is not allowed. As one moves along increasing λ_2, representing increasing polarization, we see that stability increases outside of the stability threshold and eventually decreases as electric self-interactions begin to dominate the free energy.

The effects of electric self-interaction on the stable fiber radius are illustrated by comparing Fig. 5 to Fig. 6. In Fig. 5, we see that polarization effects, such as electric self-interaction can lower the stable fiber radius. On the other hand, Fig. 6 compares the effects of $\lambda_1=c'\sin\theta/\sigma$ to $\lambda_2=c''P_o\sin\theta/\sigma$ on fiber stability when P_o is held at 10^{-3} C/m^2. What we see in Fig. 6 is that no bias on fiber stability can be seen in the λ_1 to the λ_2 directions, which confirms that a dominating effect in fiber stability is electric self-interactions. This occurs due to the fact that when c' or c'' are varied they only affect the Φ_D term; however, when the polarization is varied this also affects Φ_E as well, which fights polarization divergence.

The angular dependences can be studied by varying the layer tilt angle θ_o and the bulk polarization angle α_o. The first case inspects the SmAP/SmCP transition and the second looks at the SmCP/SmCG/SmLP transitions. Using the property values in Table I and varying only the corresponding bulk angles, we obtain the curves in Figs. 7 and 8, showing the effects of θ_o and α_o on fiber stability, respectively.

The results of these numerical calculations can be summarized as follows.

(i) The SmAP phase cannot form stable fibers via this mechanism due to a lack of out-of-plane polarization. This coincides with our experimental results, in which we were not able to form fibers of the first $SmAP_A$ material [14]. It is interesting to point out, however, that the threshold tilt decreases with increasing polarization. Therefore, if the SmAP phase has a significantly large in-plane polarization, one could form a fiber if a molecular tilt could be induced through shearing the fiber about the $\hat{\psi}$ direction.

(ii) The effect of increasing polarization in all phases is a decrease in the average fiber radius, and fibers with large polarizations ($P_o\sim 5\times 10^{-3}$ C/m^2) have a stable fiber radius below the modified Plateau-Rayleigh instability limit and would be susceptible to diameter fluctuations.

(iii) The SmCP phase does not form as stable of fiber as the SmCG and SmLP phases, as seen by the larger stable radii and the lower free energy per length in these phases as shown in Fig. 8. This may explain the observations that SmCP fibers exist only in bundles and not in single form. Since experiments clearly show that B_7 fibers are much more stable than B_2 (SmCP) fibers, this model is consistent with the possibility that the B_7 phases do indeed hold C_1 (SmCG-type) symmetries [4].

IV. CONCLUSIONS

We presented a simple theoretical model assuming constant tilt and azimuth angles of bent core molecules, but allowing the rotation of the molecular plane with respect to the tilt plane by an angle α away from the SmCP situation. We showed that nonzero α values lead to the stability of single fluid fibers. Assuming reasonable material parameters, we found the minimum stable fiber radii in the micrometer range, in agreement with the experimentally observed values. Also in agreement with experimental observations, we showed that the director tilt is necessary for fiber formation. Finally, our model can explain an experimentally observed, but so far not understood, bulk elastic term in a few kPa range.

In the future we plan to proceed in two directions. On the one hand, we will refine our model by allowing variations of the angles with respect to position. On the other hand, we will further simplify our model to find analytical expressions that will relate the stable fiber radii directly to the shape of

molecules, thus making the model physically more transparent.

ACKNOWLEDGMENTS

This work has been financially supported by the NSF FRG under Contract No. DMS-0456221. We acknowledge useful discussions with Professor Daniel Phillips, Professor Particia Bauman, and Professor Jie Shen at Purdue University, Professor Maria Carme Calderer at University of Minnesota, and Professor Jonathan Selinger at Kent State University.

[1] A. Jákli, A. Saupe, *One and Two Dimensional Fluids: Properties of Smectic, Lamellar, and Columnar Liquid Crystals* (Taylor & Francis, London, (2006), pp. 74–80.
[2] D. H. Van Winkle and N. A. Clark, Phys. Rev. Lett. **48**, 1407 (1982).
[3] J. Prost, and N. A. Clark (unpublished).
[4] A. Jákli, D. Krüerke, and G. G. Nair, Phys. Rev. E **67**, 051702 (2003).
[5] G. Pelzl, S. Diele, A. Jákli, CH. Lischka, I. Wirth, and W. Weissflog, Liq. Cryst. **26**, 135 (1999).
[6] C.-K. Lee and L. C. Chien, Liq. Cryst. **26**, 609 (1999).
[7] D. R. Link, N. Chattham, N. A. Clark, E. Körblova, and D. M. Walba (unpublished).
[8] A. Jákli, Ch. Lischka, W. Weissflog, G. Pelzl, and A. Saupe, Liq. Cryst. **27**, 1405 (2000).
[9] R. Pratibha and N. V. Madhusudana, J. Phys. II **2**, 383 (1992).
[10] A. Eremin, A. Nemes, and R. Stannarius, Phys. Rev. E **71**, 031705 (2005).
[11] A. Nemes, A. Eremin, R. Stannarius, M. Schultz, H. Nádasi, and W. Weissflog, Phys. Chem. Chem. Phys. **8**, 469 (2006).
[12] R. Stannarius, A. Nemes, and A. Eremin, Phys. Rev. E **72**, 020702(R) (2005).
[13] H. R. Brand, P. E. Cladis, and H. Pleiner, Eur. Phys. J. B **6**, 347 (1998).
[14] A. Eremin, S. Diele, G. Pelzl, H. Nadasi, W. Weissflog, J. Salfetnikova, and H. Kresse, Phys. Rev. E **64**, 051707 (2001).
[15] A. Jákli, D. Krüerke, H. Sawade, and G. Heppke, Phys. Rev. Lett. **86**, 5715 (2001).
[16] D. A. Coleman, J. Fernsler, N. Chattham, M. Nakata, Y. Takanishi, E. Körblova, D. R. Link, R.-F. Shao, W. G. Jang, J. E. Maclennan, O. Mondainn-Monval, C. Boyer, W. Weissflog, G. Pelzl, L-C. Chien, J. Zasadzinski, J. Watanabe, D. M. Walba, H. Takezoe, and N. A. Clark, Science **301**, 1204 (2003).
[17] J. Xu, R. L. B. Selinger, J. V. Selinger, and R. Shashidhar, J. Chem. Phys. **115**, 4333 (2001).
[18] P. G. de Gennes, *The Physics of Liquid Crystals* (Oxford University Press, Oxford, 1974).